

# Measurement of the Cross-Section for the Process $\gamma\gamma \rightarrow p\bar{p}$ at $\sqrt{s_{ee}} = 183 - 189$ GeV with the OPAL Detector at LEP

T. Barillari<sup>a</sup>

<sup>a</sup>Max-Planck-Institut für Physik, Werner-Heisenberg-Institut,  
Foehringer Ring 6, D-80805 Muenchen, Germany

The exclusive production of proton-antiproton pairs in the collisions of two quasi-real photons has been studied using data taken at  $\sqrt{s_{ee}} = 183$  GeV and 189 GeV with the OPAL detector at LEP. Results are presented for  $p\bar{p}$  invariant masses,  $W$ , in the range  $2.15 < W < 3.95$  GeV. The cross-section measurements are compared with previous data and with recent analytic calculations based on the quark-diquark model.

## 1. INTRODUCTION

The exclusive production of proton-antiproton ( $p\bar{p}$ ) pairs in the collision of two quasi-real photons can be used to test predictions of QCD. At LEP the photons are emitted by the beam electrons<sup>1</sup> and the  $p\bar{p}$  pairs are produced in the process  $e^+e^- \rightarrow e^+e^-\gamma\gamma \rightarrow e^+e^-p\bar{p}$ .

The application of QCD to exclusive photon-photon reactions is based on the work of Brodsky and Lepage [1]. Calculations based on this ansatz [2,3] use a specific model of the proton's three-quark wave function by Chernyak and Zhitnitsky [4]. This calculation yields cross-sections about one order of magnitude smaller than the existing experimental results [5,6,7,8,9,10,11], for  $p\bar{p}$  centre-of-mass energies  $W$  greater than 2.5 GeV.

To model non-perturbative effects, the introduction of quark-diquark systems has been proposed [12].

Recent studies [13] have extended the systematic investigation of hard exclusive reactions within the quark-diquark model to photon-photon processes [14,15,16,17].

The calculations of the integrated cross-section for the process  $\gamma\gamma \rightarrow p\bar{p}$  in the angular range  $|\cos\theta^*| < 0.6$  (where  $\theta^*$  is the angle between the proton's momentum and the electron beam direction in the  $p\bar{p}$  centre-of-mass system) and for  $W > 2.5$  GeV are in good agreement with ex-

perimental results [9,10], whereas the pure quark model predicts much smaller cross-sections [2,3].

In this paper, we present a measurement of the cross-section [11] for the exclusive process  $e^+e^- \rightarrow e^+e^-p\bar{p}$  in the range  $2.15 < W < 3.95$  GeV, using data taken with the OPAL detector [18] at  $\sqrt{s_{ee}} = 183$  GeV and 189 GeV at LEP. The integrated luminosities for the two energies are  $62.8 \text{ pb}^{-1}$  and  $186.2 \text{ pb}^{-1}$ .

## 2. EVENT SELECTION

The  $e^+e^- \rightarrow e^+e^-p\bar{p}$  events are selected by the following set of cuts:

1. The sum of the energies measured in the barrel and endcap sections of the electromagnetic calorimeter must be less than half the beam energy.
2. Exactly two oppositely charged tracks are required with each track having at least 20 hits in the central jet chamber to ensure a reliable determination of the specific energy loss  $dE/dx$ . The point of closest approach to the interaction point must be less than 1 cm in the  $r\phi$  plane and less than 50 cm in the  $z$  direction.
3. For each track the polar angle must be in the range  $|\cos\theta| < 0.75$  and the transverse momentum  $p_{\perp}$  must be larger than 0.4 GeV. These cuts ensure a high trigger efficiency and good particle identification.

<sup>1</sup>In this paper positrons are also referred to as electrons.

4. The invariant mass  $W$  of the  $p\bar{p}$  final state must be in the range  $2.15 < W < 3.95$  GeV. The invariant mass is determined from the measured momenta of the two tracks using the proton mass.
5. The events are boosted into the rest system of the measured  $p\bar{p}$  final state. The scattering angle of the tracks in this system has to satisfy  $|\cos\theta^*| < 0.6$ .
6. All events must fulfil the trigger conditions described in [11].
7. The large background from other exclusive processes, mainly the production of  $e^+e^-$ ,  $\mu^+\mu^-$ , and  $\pi^+\pi^-$  pairs, is reduced by particle identification using the specific energy loss  $dE/dx$  in the jet chamber and the energy in the electromagnetic calorimeter. The  $dE/dx$  probabilities of the tracks must be consistent with the  $p$  and  $\bar{p}$  hypothesis.

- Events where the ratio  $E/p$  for each track lies in the range  $0.4 < E/p < 1.8$  are regarded as possible  $e^+e^- \rightarrow e^+e^-e^+e^-$  candidates,  $E$  here is the energy of the ECAL cluster associated with the track with momentum  $p$ . These events are rejected if the  $dE/dx$  probabilities of the two tracks are consistent with the electron hypothesis.
- Events where the ratio  $E/p$  for each track is less than 0.8, as expected for a minimum ionizing particle, are regarded as possible background from  $e^+e^- \rightarrow e^+e^-\mu^+\mu^-$  events. This background is reduced by rejecting events where the  $dE/dx$  probability for both tracks is consistent with the muon hypothesis. This cut is also effective in reducing the  $\pi^+\pi^-$  background.
- The  $dE/dx$  probability for the proton hypothesis has to be greater than 0.1% for each track and it has to be larger than the probabilities for the pion and kaon hypotheses. The product of the  $dE/dx$  probabilities for both tracks to be (anti) protons has to be larger than

the product of the  $dE/dx$  probabilities for both tracks to be electrons.

8. Cosmic ray background is eliminated by applying a muon veto [19].
9. Exclusive two-particle final states are selected by requiring the transverse component of the momentum sum squared of the two tracks,  $|\sum \vec{p}_\perp|^2$ , to be smaller than  $0.04 \text{ GeV}^2$ . By restricting the maximum value of  $Q_i^2$ , this cut also ensures that the interacting photons are quasi-real. Therefore no further cut rejecting events with scattered electrons in the detector needs to be applied.

After all cuts 163 data events are selected, 35 events at  $\sqrt{s_{ee}} = 183$  GeV and 128 events at  $\sqrt{s_{ee}} = 189$  GeV. Background from events containing particles other than (anti-)protons is negligible due to the good rejection power of the  $dE/dx$  cuts. No event remains after applying the event selection to the background Monte Carlo samples [11]. Since the  $p\bar{p}$  final state is fully reconstructed, the experimental resolution for  $W$  (determined with Monte Carlo simulation) is better than 1%. The experimental resolution for  $|\cos\theta^*|$  is about 0.014.

### 3. CROSS-SECTION MEASUREMENTS

The differential cross-section for the process  $e^+e^- \rightarrow e^+e^-p\bar{p}$  is given by

$$\frac{d^2\sigma(e^+e^- \rightarrow e^+e^-p\bar{p})}{dW d|\cos\theta^*|} = \frac{N_{\text{ev}}(W, |\cos\theta^*|)}{\mathcal{L}_{e^+e^-} \varepsilon_{\text{TRIG}} \varepsilon_{\text{DET}}(W, |\cos\theta^*|) \Delta W \Delta|\cos\theta^*|} \quad (1)$$

where  $N_{\text{ev}}$  is the number of events selected in each  $(W, |\cos\theta^*|)$  bin,  $\varepsilon_{\text{TRIG}}$  is the trigger efficiency,  $\varepsilon_{\text{DET}}$  is the detection efficiency,  $\mathcal{L}_{e^+e^-}$  is the measured integrated luminosity, and  $\Delta W$  and  $\Delta|\cos\theta^*|$  are the bin widths in  $W$  and in  $|\cos\theta^*|$ .

The total cross-section  $\sigma(\gamma\gamma \rightarrow p\bar{p})$  for a given value of  $\sqrt{s_{ee}}$  is obtained from the differential cross-section  $d\sigma(e^+e^- \rightarrow e^+e^-p\bar{p})/dW$  using the luminosity function  $d\mathcal{L}_{\gamma\gamma}/dW$  [20]:

$$\sigma(\gamma\gamma \rightarrow p\bar{p}) = \frac{d\sigma(e^+e^- \rightarrow e^+e^-p\bar{p})}{dW} \bigg/ \frac{d\mathcal{L}_{\gamma\gamma}}{dW} \quad (2)$$

The luminosity function  $d\mathcal{L}_{\gamma\gamma}/dW$  is calculated by the GALUGA program [21]. The resulting differential cross-sections for the process  $\gamma\gamma \rightarrow p\bar{p}$  in bins of  $W$  and  $|\cos\theta^*|$  are then summed over  $|\cos\theta^*|$  to obtain the total cross-section as a function of  $W$  for  $|\cos\theta^*| < 0.6$ .

#### 4. RESULT AND DISCUSSION

The measured cross-sections [11] as a function of  $W$  are showed in Fig. 1. The average  $\langle W \rangle$  in each bin has been determined by applying the procedure described in [22]. The measured cross-sections  $\sigma(\gamma\gamma \rightarrow p\bar{p})$  for  $2.15 < W < 3.95$  GeV and for  $|\cos\theta^*| < 0.6$  are compared with the results obtained by ARGUS [8], CLEO [9] and VENUS [10] in Fig. 1a and to the results obtained by TASSO [5], JADE [6] and TPC/2 $\gamma$  [7] in Fig. 1b. The quark-diquark model predictions [13] are also shown. Reasonable agreement is found between this measurement and the results obtained by other experiments for  $W > 2.3$  GeV. At lower  $W$  our measurements agree with the measurements by JADE [6] and ARGUS [8], but lie below the results obtained by CLEO [9], and VENUS [10]. The cross-section measurements reported here extend towards higher values of  $W$  than previous results. Fig. 1c shows the measured  $\gamma\gamma \rightarrow p\bar{p}$  cross-section as a function of  $W$  together with some predictions based on the quark-diquark model [12,13]. There is good agreement between our results and the older quark-diquark model predictions [12]. The most recent calculations [13] lie above the data, but within the estimated theoretical uncertainties the predictions are in agreement with the measurement.

An important consequence of the pure quark hard scattering picture is the power law which follows from the dimensional counting rules [23,24]. The dimensional counting rules state that an exclusive cross-section at fixed angle has an energy dependence connected with the number of hadronic constituents participating in the process under investigation. We expect that for asymptotically large  $W$  and fixed  $|\cos\theta^*|$

$$\frac{d\sigma(\gamma\gamma \rightarrow p\bar{p})}{dt} \sim W^{2(2-n)} \quad (3)$$

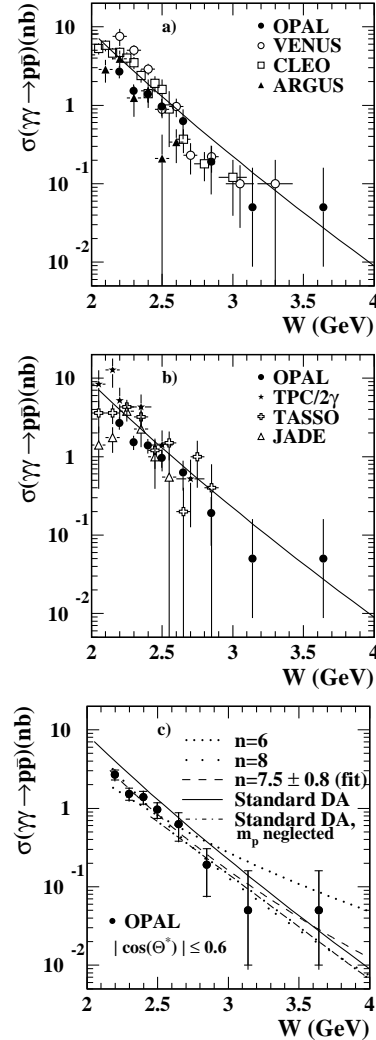


Figure 1. Cross-sections  $\sigma(\gamma\gamma \rightarrow p\bar{p})$  as a function of  $W$  for  $|\cos\theta^*| < 0.6$ . Data points are plotted at the value of  $\langle W \rangle$ . a,b) The data are compared to other experimental results [7,8,9,10] and to the quark-diquark model prediction [13]. The error bars include statistical and systematic uncertainties, except for TASSO [5] where the uncertainties are statistical only. c) The data are compared to the quark-diquark model of [12] (dash-dotted line), and of [13] (solid line), using the standard DA [12,13] with and without neglecting the mass  $m_p$  of the proton, and with the predictions of the power law with fixed and with fitted exponent  $n$ . Inner error bars are statistical uncertainties and outer error bars are total uncertainties.

where  $n = 8$  is the number of elementary fields and  $t = -W^2/2(1 - |\cos\theta^*|)$ . The introduction of diquarks modifies the power law by decreasing  $n$  to  $n = 6$ . This power law is compared to the data in Fig. 1c with  $\sigma(\gamma\gamma \rightarrow p\bar{p}) \sim W^{-2(n-3)}$  using three values of the exponent  $n$ : fixed values  $n = 8$ ,  $n = 6$ , and the fitted value  $n = 7.5 \pm 0.8$  obtained by taking into account statistical uncertainties only. More data covering a wider range of  $W$  would be required to determine the exponent  $n$  more precisely. The measured differential cross-sections  $d\sigma(\gamma\gamma \rightarrow p\bar{p})/d|\cos\theta^*|$  in different  $W$  ranges and for  $|\cos\theta^*| < 0.6$  are showed in Fig. 2. The differential cross-section in the range  $2.15 < W < 2.55$  GeV lies below the results reported by VENUS [10] and CLEO [9] (Fig. 2a). Since the CLEO measurements are given for the lower  $W$  range  $2.0 < W < 2.5$  GeV, we rescale their results by a factor 0.635 which is the ratio of the two CLEO total cross-section measurements integrated over the  $W$  ranges  $2.0 < W < 2.5$  GeV and  $2.15 < W < 2.55$  GeV. This leads to a better agreement between the two measurements but the OPAL results are still consistently lower. The shapes of the  $|\cos\theta^*|$  dependence of all measurements are consistent apart from the highest  $|\cos\theta^*|$  bin, where the OPAL measurement is significantly lower than the measurements of the other two experiments.

In Fig. 2b-c the differential cross-sections  $d\sigma(\gamma\gamma \rightarrow p\bar{p})/d|\cos\theta^*|$  in the  $W$  ranges  $2.35 < W < 2.85$  GeV and  $2.55 < W < 2.95$  GeV are compared to the measurements by TASSO, VENUS and CLEO in similar  $W$  ranges. The measurements are consistent within the uncertainties. The comparison of the differential cross-section as a function of  $|\cos\theta^*|$  for  $2.55 < W < 2.95$  GeV with the calculation of [13] at  $W = 2.8$  GeV for different distribution amplitudes (DA) is shown in Fig. 3a. The shapes of the curves of the pure quark model [2,3] and the quark-diquark model predictions [13] are consistent with those of the data.

In Fig. 3b the differential cross-section  $d\sigma(\gamma\gamma \rightarrow p\bar{p})/d|\cos\theta^*|$  is shown versus  $|\cos\theta^*|$  for  $2.15 < W < 2.55$  GeV. The cross-section decreases at large  $|\cos\theta^*|$ ; the shape of the angular distribution is different from that at higher  $W$

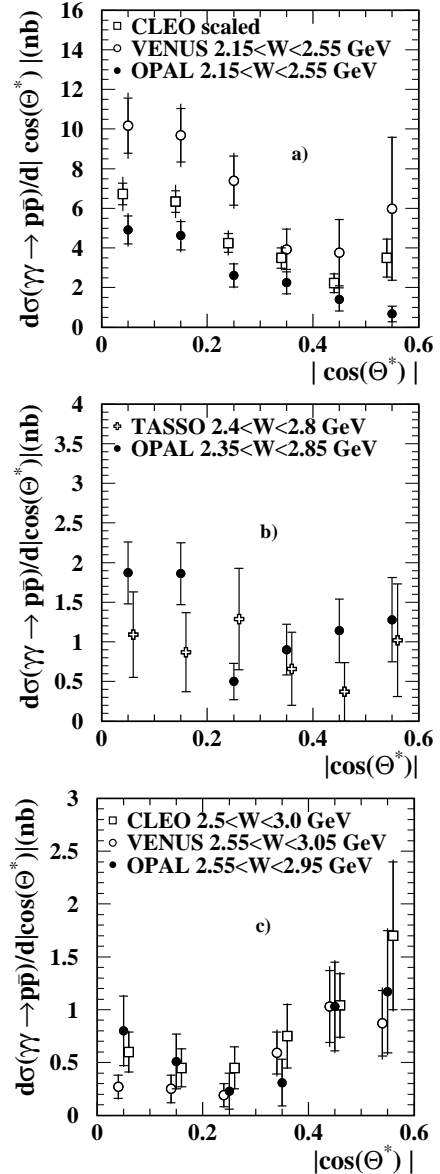


Figure 2. Differential cross-sections for  $\gamma\gamma \rightarrow p\bar{p}$  as a function of  $|\cos\theta^*|$  in different ranges of  $W$ ; a, c) compared with CLEO [9] and VENUS [10] data with statistical (inner error bars) and systematic errors (outer bars) and b) compared with TASSO [5]. The TASSO error bars are statistical only. The data points are slightly displaced for clarity.

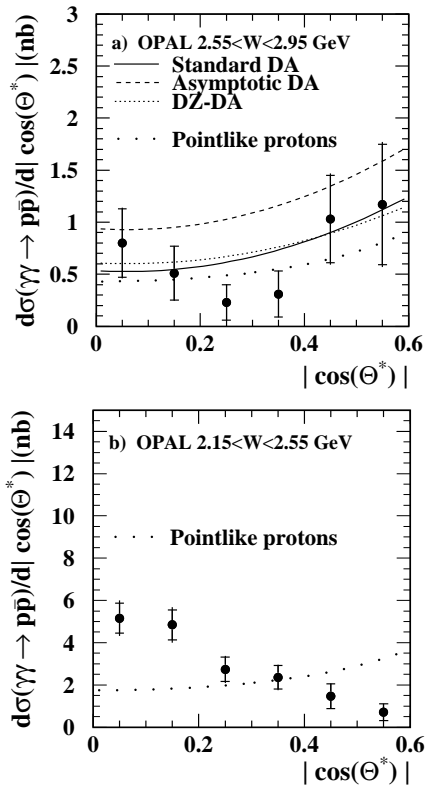


Figure 3. Measured differential cross-section,  $d\sigma(\gamma\gamma \rightarrow p\bar{p})/d|\cos\theta^*|$ , with statistical (inner bars) and total uncertainties (outer bars) for a)  $2.55 < W < 2.95$  GeV and b)  $2.15 < W < 2.55$  GeV. The data are compared with the pointlike approximation for the proton (4) scaled to fit the data. The other curves show the pure quark model [2], the diquark model of [12] with the Dziembowski distribution amplitudes (DZ-DA), and the diquark model of [13] using standard and asymptotic distribution amplitudes.

values. This indicates that for low  $W$  the perturbative calculations of [2,3] are not valid.

Another important consequence of the hard scattering picture is the hadron helicity conservation rule. For each exclusive reaction like  $\gamma\gamma \rightarrow p\bar{p}$  the sum of the two initial helicities equals the sum of the two final ones [25]. According to the simplification used in [12], only scalar diquarks are considered, and the (anti) proton carries the helicity of the single (anti) quark. Neglecting quark masses, quark and antiquark and hence proton and antiproton have to be in opposite helicity states. If the (anti) proton is considered as a point-like particle, simple QED rules determine the angular dependence of the unpolarized  $\gamma\gamma \rightarrow p\bar{p}$  differential cross-section [26]:

$$\frac{d\sigma(\gamma\gamma \rightarrow p\bar{p})}{d|\cos\theta^*|} \propto \frac{(1 + \cos^2\theta^*)}{(1 - \cos^2\theta^*)}. \quad (4)$$

This expression is compared to the data in two  $W$  ranges,  $2.55 < W < 2.95$  GeV (Fig. 3a) and  $2.15 < W < 2.55$  GeV (Fig. 3b). The normalisation in each case is determined by the best fit to the data. In the higher  $W$  range, the prediction (4) is in agreement with the data within the experimental uncertainties. In the lower  $W$  range this simple model does not describe the data. At low  $W$  soft processes such as meson exchange are expected to introduce other partial waves, so that the approximations leading to (4) become invalid [27].

## 5. CONCLUSIONS

The cross-section for the process  $e^+e^- \rightarrow e^+e^-p\bar{p}$  has been measured in the  $p\bar{p}$  centre-of-mass energy range of  $2.15 < W < 3.95$  GeV using data taken with the OPAL detector at  $\sqrt{s_{ee}} = 183$  and 189 GeV. The measurement extends to slightly larger values of  $W$  than in previous measurements.

The total cross-section  $\sigma(\gamma\gamma \rightarrow p\bar{p})$  as a function of  $W$  is obtained from the differential cross-section  $d\sigma(e^+e^- \rightarrow e^+e^-p\bar{p})/dW$  using a luminosity function. For the high  $p\bar{p}$  centre-of-mass energies,  $W > 2.3$  GeV, the measured cross-section is in good agreement with other experimental results [5,7,8,9,10]. At lower  $W$  the OPAL

measurements lie below the results obtained by CLEO [9], and VENUS [10], but agree with the JADE [6] and ARGUS [8] measurements. The cross-section as a function of  $W$  is in agreement with the quark-diquark model predictions of [12,13].

The power law fit yields an exponent  $n = 7.5 \pm 0.8$  where the uncertainty is statistical only. Within this uncertainty, the measurement is not able to distinguish between predictions for the proton to interact as a state of three quasi-free quarks or as a quark-diquark system. These predictions are based on dimensional counting rules [23,24].

The shape of the differential cross-section  $d\sigma(\gamma\gamma \rightarrow p\bar{p})/d|\cos\theta^*|$  agrees with the results of previous experiments in comparable  $W$  ranges, apart from the highest  $|\cos\theta^*|$  bin measured in the range  $2.15 < W < 2.55$  GeV. In this low  $W$  region contributions from soft processes such as meson exchange are expected to complicate the picture by introducing extra partial waves, and the shape of the measured differential cross-section  $d\sigma(\gamma\gamma \rightarrow p\bar{p})/d|\cos\theta^*|$  does not agree with the simple model that leads to the helicity conservation rule. In the high  $W$  region,  $2.55 < W < 2.95$  GeV, the experimental and theoretical differential cross-sections  $d\sigma(\gamma\gamma \rightarrow p\bar{p})/d|\cos\theta^*|$  agree, indicating that the data are consistent with the helicity conservation rule.

## REFERENCES

1. G.P. Lepage and S.J. Brodsky, Phys. Rev. D22 (1980) 2157.
2. G.R. Farrar, E. Maina and F. Neri, Nucl. Phys. B259 (1985) 702.
3. D. Millers and J.F. Gunion, Phys. Rev. D34 (1986) 2657.
4. V.L. Chernyak and I.R. Zhitnitsky, Nucl. Phys. B246 (1984) 52.
5. TASSO Collaboration, M. Althoff et al., Phys. Lett. B130 (1983) 449.
6. JADE Collaboration, W. Bartel et al., Phys. Lett. B174 (1986) 350.
7. TPC/Two Gamma Collaboration, H. Aihara et al., Phys. Rev. D36 (1987) 3506.
8. ARGUS Collaboration, H. Albrecht et al., Z. Phys. C42 (1989) 543.
9. CLEO Collaboration, M. Artuso et al., Phys. Rev. D50 (1994) 5484.
10. VENUS Collaboration, H. Hamasaki et al., Phys. Lett. B407 (1997) 185.
11. OPAL Collaboration, G. Abbiendi et al., Eur. Phys. J. C28 (2003) 45.
12. M. Anselmino, P. Kroll and B. Pire, Z. Phys. C36 (1987) 89.
13. C.F. Berger, B. Lechner and W. Schweiger, Fizika B8 (1999) 371.
14. M. Anselmino, F. Caruso, P. Kroll and W. Schweiger, Int. J. Mod. Phys. A4 (1989) 5213.
15. P. Kroll, M. Schürmann and W. Schweiger, Int. J. Mod. Phys. A6 (1991) 4107.
16. P. Kroll, Th. Pilsner, M. Schürmann and W. Schweiger, Phys. Lett. B316 (1993) 546.
17. P. Kroll, M. Schürmann and P.A.M. Guichon, Nucl. Phys. A598 (1996) 435.
18. OPAL Collaboration, K. Ahmet et al., Nucl. Instr. Meth. A305 (1991) 275;
19. R. Akers et al., Z. Phys. C65 (1995) 47.
20. F.E. Low, Phys. Rev. 120 (1960) 582.
21. G.A. Schuler, Comp. Phys. Comm. 108 (1998) 279.
22. G.D. Lafferty, T.R. Wyatt, Nucl. Instr. Meth. A355 (1995) 541.
23. S.J. Brodsky and G.R. Farrar, Phys. Rev. Lett. 31 (1973) 1153.
24. V.A. Matveev, R.M. Muradian and A.N. Tavkhelidze, Nuovo Cim. Lett. 7 (1973) 719.
25. S.J. Brodsky and G.P. Lepage, Phys. Rev. D24 (1981) 2848.
26. V.M. Budnev, I.F. Ginzburg, G.V. Meledin and V.G. Serbo, Phys. Rep. 15 (1974) 181.
27. S.J. Brodsky, F.C. Ern e, P.H. Damgaard and P.M. Zerwas, Contribution to ECFA Workshop LEP200, Aachen, Germany, Sep 29 - Oct 1, 1986.